Materials Science & Engineering A 568 (2013) 176–183

Contents lists available at SciVerse ScienceDirect

Materials Science & Engineering A

journal homepage: www.elsevier.com/locate/msea

Strain-induced refinement and thermal stability of a nanocrystalline steel produced by surface mechanical attrition treatment

W.B. Liu [a], C. Zhang [a,*], Z.X. Xia [b], Z.G. Yang [a], P.H. Wang [c], J.M. Chen [c]

[a] Key Laboratory of Advanced Materials of Ministry of Education, Department of Materials Science and Engineering, Tsinghua University, Beijing 100084, China
[b] Suzhou Nuclear Power Research Institute, Suzhou 215004, China
[c] Southwestern Institute of Physics, Chengdu 610041, China

ARTICLE INFO

Article history:
Received 23 August 2012
Received in revised form
11 December 2012
Accepted 13 December 2012
Available online 12 January 2013

Keywords:
Nanocrystalline materials
Surface mechanical attrition treatment
Grain refinement
Thermal stability

ABSTRACT

A surface layer with a depth-dependent nanocrystalline microstructure was formed on reduced activation ferrite-martensitic (RAFM) steel by means of surface mechanical attrition treatment (SMAT). Equiaxed nano-sized grains in the surface layer were characterized by XRD, SEM and TEM, and the result indicated that the grain size decreased gradually with increasing deformation strain and strain rate. Compared with the size and number of carbides in the matrix, smaller and fewer carbides were detected in the SMAT layer, which indicated the refining and dissolving process of carbide during the drastic deformation in the SMAT process. Sub-grain boundaries (sub-GB) and high dense dislocation walls (DDWs) in ferrite were found in deformation layer, and dislocation accumulation, rearrangement and annihilation during the drastic deformation were discussed in detail. Both TEM images and XRD results demonstrate that the nanocrystalline layer has excellent thermal stability after annealing at 823 K.

1. Introduction

It is well known that nanocrystalline (NC) materials exhibit many excellent properties relative to the coarse-grained counterparts [1]. Plastic deformation has proved to be an effective way to refine microstructure of alloys and metals [2]. In the past decade, severe plastic deformation (SPD) methods, including ultrasonic shot peening (USP) [3–5], high-energy shot peening (HESP) [6], fast multiple rotation rolling (FMRR) [7], surface mechanical grinding treatment (SMGT) [8] and surface mechanical attrition treatment (SMAT) [9], have attracted growing interest and have been put forward.

Among the mentioned methods, SMAT is regarded to be novel and efficient technique to achieve bulk NC surface layer with gradient distribution of grain sizes along the depth. Many materials, including pure metals [10] and alloys [11], have been explored experimentally. A comprehensive understanding of grain refinement mechanism [12], element diffusion in nano-grain boundaries [13,14] and microstructure evolution along depth [15,16] have been achieved in which dislocation activities and phase transformations are found to make a key role. Annealing behaviors [17] and austenitization processes [18] in a nanocrystalline ferritic steel are also investigated.

Reduced activation ferrite/martensite (RAFM) steels are under consideration for certain nuclear fusion related applications [19]. Compared with other low-alloy steels, the kinetics of carbide precipitation in 12Cr1MoV steels are rapid because of the large concentrations of carbide-forming substitutional solutes [20,21]. Studies about SMAT in steel with spheroidal cementite particles showed that the detectable amount of cementite decreases with a decrease in depth (increasing strain), and cementite particles absolutely decomposed in the topmost surface [15]. Lu et al. [13,22] studied the chromizing process in the SMAT surface layer of low carbon steels, and the results showed that the nanostructures are effectively stabilized by the formation of fine dispersive Cr compound particles. It is not clear, however, whether chromium contained carbides would decompose during SMAT process. Therefore, the investigation of dissolution of carbides during SMAT and thermal stability of nanocrystalline is essential and meaningful.

In this work, a nano-structured surface layer with a depth-depended nanocrystalline microstructure is synthesized on a RAFM steel by means of SMAT. The SMAT process produces a gradient plastic strain in the surface layer from the treated surface to the strain-free matrix. XRD, SEM and TEM are used to investigate the microstructure and carbides in the steel. The nanostructured RAFM steel was annealed at 823 K for different times to make clear the thermal stability of nano-grain.

2. Experimental

The material used in the present investigation was RAFM steel with chemical composition (in wt%): 0.12% C, 0.51% Mn, 8.50% Cr,

* Corresponding author. Tel.: +86 10 62797603; fax: +86 10 62771160.
E-mail address: chizhang@tsinghua.edu.cn (C. Zhang).

0921-5093/$ - see front matter © 2013 Elsevier B.V. All rights reserved.
http://dx.doi.org/10.1016/j.msea.2012.12.090

0.10% Ta, 1.50% W, 0.25% V and balance Fe. Heat treatment included austenitizing at 1253 K for 45 min, followed by water quenching (WQ), and then tempering at 1033 K for 90 min. The plate sample (ϕ50 × 4.0 mm in size) of the annealing steel was submitted to SMAT, the equipment and procedure of SMAT are discussed somewhere else [6,10]. The ball size was 5 mm in diameter. The vibration frequency of the chamber was 20 kHz, and the plate was treated for 30 min. Samples subjected to SMAT were annealed at 823 K for 5min, 30 min and 120 min to investigate the thermal stability. To avoid being oxidized, all the samples for annealing treatment were sealed in glass tubes with 0.3 atmosphere of argon.

X-ray diffraction (XRD) analysis of the surface layer was carried out on a Rigaku/ SMART Lab X-ray diffractometer, with Cu K_α radiation. Step length of 0.02° and 2θ ranged from 20° to 100° were taken to measure the intensity of each Bragg diffraction to evaluate the volume fraction of retained austenite before and after SMAT. Average grain size in the topmost surface was calculated in the step scanning mode, and the bcc Fe (200) and (211) Bragg diffraction peak was selected. The step size and the step time were 0.01°and 2 s, respectively. And the scanning range of diffraction angle were 62–66.5°and 79–84.5°, respectively.

Cross-sectional observation of the treated sample was performed on scanning electron microscopy (SEM) of type JEOL JSM-7001F. The samples were ground and mechanically polished in the standard manner. The polished samples were etched in a particular solution (12 ml alcohol+3 ml hydrochloric acid+1 g ferric trichloride) to obtain the microstructure and morphology of matrix and treated surface layer. Microstructure of the treated surface layer was characterized by transmission electron microscopy (TEM) on JEOL JEM-2011 and Tecnai G2 20. The TEM samples were obtained by means of cutting, grinding and thinning from the non-treated side at low temperatures.

3. Result and discussion

3.1. XRD study of surface layer

Fig. 1 shows the XRD profiles of the surface layers before and after SMAT steel. It is clear that both the annealing and SMAT samples consist of only bcc martensite (Fig. 1(a)). However, similar study about Fe–30 wt% Ni showed that stain-induced martensite formed from retained austenite during SMAT [23]. In this work, it seems hard to determine whether the transformation is necessary because there are no retained austenite existed before SMAT.

XRD pattern also shows some little peaks between 35° and 43° before and after SMAT (Fig. 1(b)). The diffraction angles are 37.81° and 41.62°, and the 2 peaks can be further determined as peaks of $Cr_{23}C_6$ (420) and (422). And the lattice parameter of $Cr_{23}C_6$ (FCC structure) is 1.06307 nm in the present work, which is a little smaller than the value of 1.0658 ± 0.001 nm of pure $Cr_{23}C_6$ in literature [24]. And this phenomenon may be attributed to the introduction of Fe into the lattice of $Cr_{23}C_6$, which can reduce the lattice constant [25]. Another worth noting information is the peaks of $Cr_{23}C_6$ become wider and weaker after SMAT, which indicates the dissolving of $Cr_{23}C_6$ carbide during SMAT. And details for this are discussed later.

Average grain size can be calculated by Scherrer–Wilson equation [26]. The average crystallite size in the SMAT surface layer were derived from the breadths at half maximum intensity of measured bcc Fe (200) and (211) peak. The crystallite size of SMAT sample is 16.4 nm, which obviously demonstrate that the average grain size is effectively refined into nanometer scale.

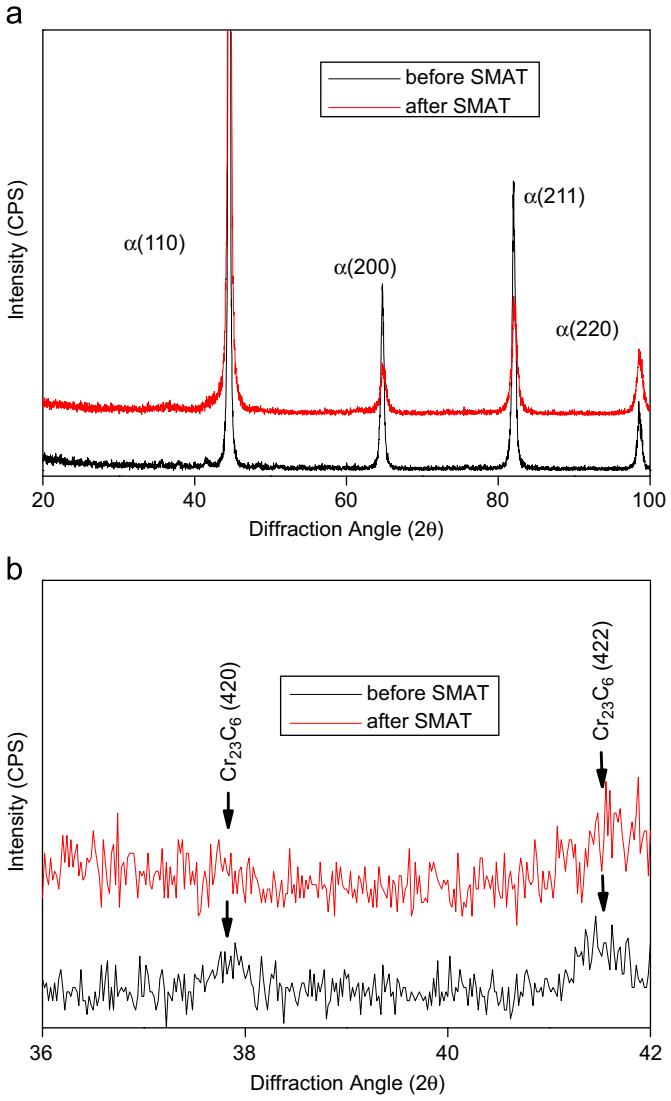

Fig. 1. XRD profiles of the surface layers before and after SMAT (a) diffraction angles from 20° to 100° and (b) detail information between diffraction angles from 36° to 42°.

3.2. Microstructure characterization

Cross-sectional morphology of the SMAT sample is shown in Fig. 2, from which severe plastic deformation can be clearly seen in the as-treated surface. Thickness of drastic deformation layer is 11–16 μm, and the reasons for this non-uniform distribution may be attributed to the heterogeneous nature of the plastic deformation within and between grains [27].

Cross-sectional SEM observations of the surface layer and matrix are shown in Fig. 3, respectively. Obviously, microstructure in surface layer is distinct from that in the deep matrix. It can be seen both the grain size and carbide distribution are uniform in the matrix. However, a gradient nano-submicro-microstructure, with increasing depth from the treated surface, is found due to the decreasing strain and strain rate, which will be further discussed in the next section by TEM. Compared with the size and number of carbides in the matrix, smaller and fewer carbides were detected in the SMAT layer (Fig. 3(a)), which indicated the refining and dissolving process of carbide during the drastic deformation in the SMAT process.

Composition analysis by energy dispersive spectrometer (EDS) in SEM for points A, B and C, which are clearly marked in Fig. 3(a),